

ANALYSIS OF THE TWO-REGIME METHOD ON SQUARE MESHES

MARK B. FLEGG*, S. JONATHAN CHAPMAN* , LIKUN ZHENG†, AND
RADEK ERBAN*

Abstract. The two-regime method (TRM) has been recently developed for optimizing stochastic reaction-diffusion simulations [11]. It is a multiscale (hybrid) algorithm which uses stochastic reaction-diffusion models with different levels of detail in different parts of the computational domain. The coupling condition on the interface between different modelling regimes of the TRM was previously derived for one-dimensional models. In this paper, the TRM is generalized to higher dimensional reaction-diffusion systems. Coupling Brownian dynamics models with compartment-based models on regular (square) two-dimensional lattices is studied in detail. In this case, the interface between different modelling regimes contain either flat parts or right-angled corners. Both cases are studied in the paper. For flat interfaces, it is shown that the one-dimensional theory can be used along the line perpendicular to the TRM interface. In the direction tangential to the interface, two choices of the TRM parameters are presented. Their applicability depends on the compartment size and the time step used in the molecular-based regime. The two-dimensional generalization of the TRM is also discussed in the case of corners.

Key words. stochastic reaction-diffusion simulations, two-regime method, multiscale modelling

AMS subject classifications. 92C40, 82C31, 60G50, 80A30

1. Introduction. There are two common approaches to stochastic reaction-diffusion modelling: (i) compartment-based models; and (ii) molecular-based models [8, 7]. Molecular-based models provide a higher level of detail, but they are often more computationally intensive than compartment-based models. In some applications, microscopic detail is only required in a relatively small region, for example, close to the cellular membrane or a particular organelle [12, 9]. Such problems are best simulated by a hybrid method which uses a detailed modelling approach in localized regions of particular interest (in which accuracy and microscopic detail is important) and a less detailed model in other regions in which accuracy may be traded for simulation efficiency. To apply this general idea to stochastic reaction-diffusion modelling, one has to introduce a suitable boundary condition between different modelling regimes. In [11], we derived the appropriate boundary condition for coupling one-dimensional compartment-based and molecular-based models. We developed the two-regime method (TRM) which has the accuracy of the detailed molecular-based approach (in the region where it is required), but benefits from the efficiency of a less detailed (coarser) compartment-based model in other parts of the computational domain. In this paper, we generalize the TRM to higher dimensional simulations.

In the remainder of this first section, we introduce the notation which is used during the rest of this manuscript. We summarize both compartment-based (Section 1.1) and molecular-based modelling (Section 1.2). Then we introduce the TRM in Section 1.3. Our main results are presented and derived in Section 2. In Section 3, we demonstrate the applicability of the presented theory using several illustrative numerical examples. Finally, we discuss other multiscale (hybrid) stochastic reaction-diffusion approaches from the literature. These methods vary in implementation and applicability and we put them into context against the TRM in Section 4.

*Mathematical Institute, University of Oxford, 24-29 St. Giles', Oxford, OX1 3LB, United Kingdom; e-mails: flegg@maths.ox.ac.uk, chapman@maths.ox.ac.uk, erban@maths.ox.ac.uk

†Department of Mathematics, University of California, Irvine, 540-N, Rowland Hall, Irvine, CA 92697, USA; e-mail: likunz@uci.edu

1.1. Compartment-based modelling. Mesoscale compartment-based modelling of reaction-diffusion processes begins by partitioning the domain Ω_C into compartments (open sets) \mathcal{C}_j , $j = 1, \dots, K$, such that the compartments do not overlap and they cover the whole domain Ω_C (i.e. $\cup_{j=1}^K \overline{\mathcal{C}_j} = \Omega_C$ and $\mathcal{C}_i \cap \mathcal{C}_j = \emptyset$, for $i \neq j$, where overbars denote the closure of the corresponding set). Assuming that there are M chemical species \mathcal{Z}_i , $i = 1, \dots, M$, the state of the system is completely defined by the copy numbers $\mathcal{N}_{i,j} \in \mathbb{N}_0$ of molecules for chemical species \mathcal{Z}_i found in the compartment \mathcal{C}_j , $i = 1, \dots, M$, $j = 1, \dots, K$. In what follows, symbol \mathbb{N}_0 denotes the set of nonnegative integers, i.e. $\mathbb{N}_0 \equiv \{0, 1, 2, 3, \dots\}$. The simulation of reaction and diffusion of the molecules in the system is usually implemented by event-driven algorithms, which include the Gillespie algorithm [17], the Next Reaction Method [16] or the Next Subvolume Method [20]. They have been implemented in several open-source software packages including MesoRD [20], URDME [5], STEPS [31] and SmartCell [2]. In this paper, we will use a derivative of the Next Reaction Method from Gibson and Bruck [16].

Event-driven algorithms require the calculation of event propensities for a particular system state [17]. An event propensity $\alpha_{\mathcal{E}}$ is the rate (per unit time) for an event \mathcal{E} to occur that changes the state of the system. Events in compartment-based reaction-diffusion processes may include: reaction events (in which chemical molecules of some species change into molecules of other species, or are just introduced or removed from the system), diffusive events (in which molecules of a chemical species jump from one compartment to an adjacent compartment) or boundary events (in which molecules are absorbed by, react with or reflect from a domain boundary). A putative time $t_{\mathcal{E}}$ for each event \mathcal{E} can be found given some current time t using

$$t_{\mathcal{E}} = t + \frac{1}{\alpha_{\mathcal{E}}} \ln \left(\frac{1}{r_{\mathcal{E}}} \right), \quad (1.1)$$

where $r_{\mathcal{E}}$ are uniformly distributed random numbers between 0 and 1 chosen separately for each occurrence of each event. The next event which takes place in the system is determined by finding which event corresponds to time $\min_{\mathcal{E}} t_{\mathcal{E}}$ where the minimum is taken over the set of all possible events [16]. The state is changed to reflect the occurrence of the event and the current time is then updated to $t := \min_{\mathcal{E}} t_{\mathcal{E}}$. The current event might also change propensities of some related events. The putative times for these events must therefore be scaled to reflect the change in propensity. That is,

$$t_{\mathcal{E}}^{\text{new}} := t + \frac{\alpha_{\mathcal{E}}^{\text{old}}}{\alpha_{\mathcal{E}}^{\text{new}}} (t_{\mathcal{E}}^{\text{old}} - t), \quad (1.2)$$

where $\alpha_{\mathcal{E}}^{\text{old}}$ and $\alpha_{\mathcal{E}}^{\text{new}}$ (resp. $t_{\mathcal{E}}^{\text{old}}$ and $t_{\mathcal{E}}^{\text{new}}$) are the propensities (resp. putative times) for event \mathcal{E} before and after the current event takes place [16]. A putative time for the next occurrence of the current event must be resampled using formula (1.1). The simulation is then constructed by a series of successive events over time, in each instance, defined by the most imminent event and performing the state change that defines that event.

1.1.1. Reaction events. One of the main assumptions of compartment modelling of stochastic reaction-diffusion models is that each compartment is small enough that it may be considered well mixed [8]. Reactions are modelled in each compartment by defining the propensity for reaction in each compartment. Consider the reaction

TABLE 1.1

Examples of propensities and effects of reactions in compartments. To simplify this table, we omit species with zero coefficients in reaction and product complexes which were included in the general form (1.3).

example reaction \mathcal{R}	$\alpha_{\mathcal{R},j}$	changes of the state vector
$\mathcal{Z}_i + \mathcal{Z}_k \xrightarrow{\kappa} \mathcal{Z}_l$	$\frac{\kappa \mathcal{N}_{i,j} \mathcal{N}_{k,j}}{V_j}$	$\mathcal{N}_{i,j}$ changes to $\mathcal{N}_{i,j} - 1$ $\mathcal{N}_{k,j}$ changes to $\mathcal{N}_{k,j} - 1$ $\mathcal{N}_{l,j}$ changes to $\mathcal{N}_{l,j} + 1$
$2\mathcal{Z}_i \xrightarrow{\kappa} \mathcal{Z}_l$	$\frac{\kappa \mathcal{N}_{i,j} (\mathcal{N}_{i,j} - 1)}{V_j}$	$\mathcal{N}_{i,j}$ changes to $\mathcal{N}_{i,j} - 2$ $\mathcal{N}_{l,j}$ changes to $\mathcal{N}_{l,j} + 1$
$\mathcal{Z}_i \xrightarrow{\kappa} \mathcal{Z}_k + \mathcal{Z}_l$	$\kappa \mathcal{N}_{i,j}$	$\mathcal{N}_{i,j}$ changes to $\mathcal{N}_{i,j} - 1$ $\mathcal{N}_{k,j}$ changes to $\mathcal{N}_{k,j} + 1$ $\mathcal{N}_{l,j}$ changes to $\mathcal{N}_{l,j} + 1$
$\emptyset \xrightarrow{\kappa} \mathcal{Z}_l$	κV_j	$\mathcal{N}_{l,j}$ changes to $\mathcal{N}_{l,j} + 1$

\mathcal{R} in compartment \mathcal{C}_j given by the general form

$$\sum_{i=1}^M \beta_i \mathcal{Z}_i \xrightarrow{\kappa} \sum_{i=1}^M \gamma_i \mathcal{Z}_i, \quad (1.3)$$

where $\beta_i \in \mathbb{N}_0$ (resp. $\gamma_i \in \mathbb{N}_0$) are the numbers of molecules of chemical \mathcal{Z}_i , $i = 1, 2, \dots, M$, that are required as reactants (resp. products) of the chemical reaction \mathcal{R} and κ is the reaction rate. We define the notation for this event $\mathcal{E} = (\mathcal{R}, j)$. In realizing this reaction event in the j -th compartment, the number of molecules $\mathcal{N}_{i,j}$, $i = 1, 2, \dots, M$, $j = 1, 2, \dots, K$, change by the corresponding stoichiometric coefficient $\nu_i = \gamma_i - \beta_i$. Considering mass action chemical kinetics, the propensity for this event to occur depends on the number of available reactants in the compartment \mathcal{C}_j . In 3D, we can postulate this dependence in the following form [8, 7]

$$\alpha_{\mathcal{R},j} = \kappa V_j^{1-\sum_i \beta_i} \prod_{i=1}^M \frac{\mathcal{N}_{i,j}!}{(\mathcal{N}_{i,j} - \beta_i)!} \quad (1.4)$$

where V_j is the volume of the compartment \mathcal{C}_j . Table 1.1 shows the examples of propensity $\alpha_{\mathcal{R},j}$ for some simple reactions \mathcal{R} in compartment \mathcal{C}_j and the subsequent changes to the state of the system that occur as a result of the reaction event.

The main focus of this paper is on 2D simulations. In this case, the formula (1.4) has to be slightly modified by replacing the compartment volume V_j by its area. Since the propensity $\alpha_{\mathcal{R},j}$ is dimensionless, some rate constants have different physical units in 2D than in 3D. In applications, 2D simulations in the domain $\Omega_C \subset \mathbb{R}^2$ are often viewed as a model of a real 3D domain $\Omega_C \times (0, w)$ where the domain width w is so small that the spatial distribution along the third axis can be neglected. Then the formula (1.4) can be applied with the standard interpretation (i.e. physical units) of the reaction rates. The area of each 2D compartment is multiplied by w to get the corresponding volume V_j in (1.4).

1.1.2. Diffusion events. Diffusion in compartment-based models of reaction-diffusion processes is defined by the stochastic jumping of molecules of chemical species

\mathcal{Z}_i , $i = 1, 2, \dots, M$, between any two adjacent compartments from \mathcal{C}_j to \mathcal{C}_k , $j, k = 1, 2, \dots, K$. We shall define the notation for this diffusive event to be $\mathcal{E} = (\mathcal{D}, i, j, k)$. The propensity for a diffusive event is given by

$$\alpha_{\mathcal{D}, i, j, k} = q_{j, k} D_i \mathcal{N}_{i, j}, \quad (1.5)$$

where $q_{j, k}$ is dependent on the morphology and relative positions of the compartments \mathcal{C}_j and \mathcal{C}_k , and D_i is the diffusion constant for chemical \mathcal{Z}_i . For adjacent square or cubic compartments \mathcal{C}_j and \mathcal{C}_k of length h on a regular lattice, we have $q_{j, k} = 1/h^2$, i.e.

$$\alpha_{\mathcal{D}, i, j, k} = \frac{D_i}{h^2} \mathcal{N}_{i, j}, \quad (1.6)$$

and $q_{j, k} = 0$ if \mathcal{C}_j and \mathcal{C}_k do not share a common side. For more irregular compartment shapes, $q_{j, k}$ can be determined by the finite element discretisation of the diffusion equation on a lattice whose vertices are at the centers of the compartments [5]. During the diffusive event (\mathcal{D}, i, j, k) , the state of the system is changed to reflect the movement of one molecule of \mathcal{Z}_i from \mathcal{C}_j to \mathcal{C}_k , i.e. $\mathcal{N}_{i, j}$ changes to $\mathcal{N}_{i, j} - 1$ and $\mathcal{N}_{i, k}$ changes to $\mathcal{N}_{i, k} + 1$.

1.1.3. Boundary events. Boundary events are caused by the diffusion of molecules into the boundaries of the domain $\partial\Omega_C$. It is no surprise then that boundary events are linked closely to diffusion events. Consider the compartment \mathcal{C}_j which is adjacent to $\partial\Omega_C$. A diffusive event of a molecule of chemical \mathcal{Z}_i which would ordinarily result in a jump from \mathcal{C}_j to a compartment on the other side of $\partial\Omega_C$ actually results in an interaction of the molecule with the boundary. Such an interaction usually results in one of two outcomes either: the molecule is absorbed; or the molecule is reflected [6]. Molecules attached to the surface can be released back into the solution [3, 23]. However, in this paper, we will consider reflective boundary conditions on all external boundaries for simplicity.

1.2. Molecular-based modelling. Molecular-based approaches to reaction-diffusion modelling are characterized by the prescription of exact coordinates in space for each molecule of each chemical species \mathcal{Z}_i , $i = 1, 2, \dots, M$, in the continuous domain $\Omega_M \subset \mathbb{R}^N$, where $N = 1, 2, 3$. The trajectory of large molecules (such as proteins) are computed using Brownian dynamics [4, 14, 28]. A random displacement of each molecule every timestep Δt models the effect of solvent molecules on the large molecules of interest without the need to simulate each solvent molecule individually. We will denote the j -th molecule of chemical species \mathcal{Z}_i as Z_i^j . Given a time step Δt the position $\mathbf{x}_{i, j}(t + \Delta t)$ of molecule Z_i^j at time $t + \Delta t$ is computed from its position $\mathbf{x}_{i, j}(t)$ at time t in the N -dimensional continuous space Ω_M by

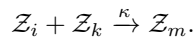
$$\mathbf{x}_{i, j}(t + \Delta t) = \mathbf{x}_{i, j}(t) + \sqrt{2D_i \Delta t} \boldsymbol{\zeta}, \quad (1.7)$$

where $\boldsymbol{\zeta} \in \mathbb{R}^N$ is a vector of N uncorrelated normally distributed random numbers with zero mean and unit variance chosen separately for each molecule. The equation (1.7) is a discretization of the standard Brownian motion

$$d\mathbf{X}_{i, j} = \sqrt{2D_i} d\mathbf{W}_{i, j}. \quad (1.8)$$

Molecular-based models have been implemented in several software packages, including Smoldyn [4], MCell [26] and GFRD [29]. They have been used for modelling several biological systems, including the signal transduction in bacterium *E. coli* [24] and the MAPK pathway [27].

1.2.1. Chemical reactions. It is relatively straightforward to implement zero-order and first-order chemical reactions in molecular-based models [8]. There is a variety of different ways to model bimolecular (second-order) molecular-based reactions. Consider two molecules Z_i^j and Z_k^l which can react according to the following bimolecular reaction



Then a suitable probability of reaction per time step is chosen such that the macroscopic rate of reaction between the two chemicals is κ [7]. This probability is a function of the distance $|\mathbf{x}_{i,j} - \mathbf{x}_{k,l}|$ between reacting molecules. Models postulate that the molecules can only react if they are within a specific distance (reaction radius) [4]. Care must also be taken when generating the initial positions of products of chemical reactions. This is especially the case whenever reversible reactions are present in the system. If the molecules are not initialized properly then the products may unphysically react immediately after being created [23, 21].

1.2.2. Boundary conditions. Molecules that migrate over domain boundaries are treated depending on whether they are reflective, absorbing or reactive boundaries [6]. When modelling boundary conditions, one has to take into account that (1.7) is only an approximation of the Brownian motion (1.8). Let us consider that the formula (1.7) gives the updated position of the molecule Z_i^j inside the domain Ω_M , i.e. $\mathbf{x}_{i,j}(t + \Delta t) \in \Omega_M$. Then there is still a nonzero probability that the molecule (which follows (1.8)) left the domain Ω_M during the time $(t, t + \Delta t)$ and then returned back to Ω_M . We denote this probability by $P_m \equiv P_m(\mathbf{x}_{i,j}(t), \mathbf{x}_{i,j}(t + \Delta t))$. Near a flat boundary $\partial\Omega_M$, probability P_m takes the analytical form

$$P_m = \exp\left(\frac{-\text{dist}(\mathbf{x}_{i,j}(t), \partial\Omega_M) \text{dist}(\mathbf{x}_{i,j}(t + \Delta t), \partial\Omega_M)}{D_i \Delta t}\right), \quad (1.9)$$

where $\text{dist}(\cdot, \partial\Omega_M)$ represents the distance from the boundary $\partial\Omega_M$ [4]. Whilst boundaries are sometimes only implemented at time $t + \Delta t$ for molecule Z_i^j if $\mathbf{x}_{i,j}(t + \Delta t)$ computed by (1.7) is outside Ω_M , thorough implementation of boundary conditions should not only be considered when $\mathbf{x}_{i,j}(t + \Delta t) \notin \Omega_M$ but also with the probability P_m if $\mathbf{x}_{i,j}(t + \Delta t) \in \Omega_M$. No closed form solution exists for P_m for irregular boundary geometries $\partial\Omega_M$. In practice, a curved boundary is usually described locally by a flat approximation which increasingly becomes more accurate for small values of Δt [4].

1.3. The two-regime method. Molecular-based techniques are usually preferred over compartment-based simulation techniques when the concentration of molecules is low to give a level of microscopic detail that is not achievable in the mesoscopic compartment-based approaches. However, it can be very cumbersome numerically to simulate every single molecule and perform probability tests for every pair of molecules that have the potential to react if the copy numbers of molecular species are large. In such cases, compartment-based approaches are appropriate. They provide a level of efficiency that does not require the tracking of each individual molecule. This comes, however, at the cost of detail in the simulation. This paper focuses on the TRM which provides a way to spatially connect regions that use compartment-based modelling in regions that require a mesoscopic level of detail with that of molecular-based modelling in regions where the concentrations are lower or a high level of detail is required [11].

The TRM for simulation of stochastic reaction-diffusion processes is characterized by its partition of the computational domain $\Omega \subset \mathbb{R}^N$, $N = 1, 2, 3$, into two non-overlapping open subsets Ω_C and Ω_M , i.e. $\Omega_C \cap \Omega_M = \emptyset$ and $\overline{\Omega_C} \cup \overline{\Omega_M} = \overline{\Omega}$ where overbars denote the closure of the corresponding set. We denote by I the interface between the subdomains Ω_C and Ω_M , i.e. $I = \partial\Omega_C \cap \partial\Omega_M$. Internally, molecules are simulated in subdomains Ω_C and Ω_M by compartment-based and molecular-based approaches which were described in Sections 1.1 and 1.2, respectively. Molecules in Ω_M are updated at prescribed times separated by Δt . Meanwhile, molecules in Ω_C are updated at the events determined by compartment modelling rules described in Section 1.1. The simulation is thus built from a series of time steps that occur at each “regular time step” separated by Δt and each event inside Ω_C . As the time updates can be classified by the region that they apply to, updates corresponding to compartment-based events are known as C -events (or compartment events) and the regular updates separated by Δt in time are known as M -events. There are several possible variants of the TRM [11]. In this paper, we will analyse the TRM in the form which is summarized in Table 1.2. In the step (i), we define Ω_C , Ω_M and the time step Δt . Initial conditions in Ω_M and Ω_C are implemented in the steps (ii) and (iii), respectively. In the step (iv), we also define putative times t_M and t_C when the next M -event and C -event will occur, respectively. Then the TRM repeats steps (v) and (vi) until the desired end of the simulation.

1.3.1. Transition of molecules from Ω_C to Ω_M . The partition of the domain into Ω_C and Ω_M is an artificial partitioning that should not interfere with the natural diffusion of molecules in the domain. To describe migration of molecules from Ω_C to Ω_M , we need an expression for the propensity of molecules to jump from compartments \mathcal{C}_j , adjacent to the interface I , into Ω_M . When a molecule successfully jumps from \mathcal{C}_j into Ω_M , it must be placed with a specific set of coordinates by virtue of the modelling approach in Ω_M . For a regular array of square or cubic compartments in Ω_C , we define the propensity of chemical species \mathcal{Z}_i to jump from \mathcal{C}_j into Ω_M to be some multiple $\Phi_{i,j}$ times the natural jumping propensity between neighbouring compartments (provided that compartment \mathcal{C}_j is adjacent to I , a so-called *interfacial compartment*, otherwise this propensity is equal to 0). That is (compare with (1.6)),

$$\alpha_{\mathcal{D},i,j,M} = \Phi_{i,j} \frac{D_i}{h^2} \mathcal{N}_{i,j}, \quad (1.10)$$

where the index j is a reference to the originating interfacial compartment \mathcal{C}_j . Subsequently, the molecule, after being chosen to jump from \mathcal{C}_j into Ω_M is initialized at a position $\mathbf{x} \in \Omega_M$. We do not restrict this initialization to a specific location but rather consider that the initial position is chosen from a probability distribution $f_{i,j}(\mathbf{x})$.

1.3.2. Transition of molecules from Ω_M to Ω_C . In step (vi), a molecule originating in Ω_M is transferred into Ω_C with a probability $\Psi \in [0, 1]$ if the molecule interacted with the interface I within the time interval $[t, t + \Delta t]$. It is postulated that molecule \mathcal{Z}_i^j interacted with I if one of these two conditions is satisfied:

- (a) $\mathbf{x}_{i,j}(t + \Delta t)$ computed by (1.7) satisfies $\mathbf{x}_{i,j}(t + \Delta t) \in \Omega_C$;
 - (b) $\mathbf{x}_{i,j}(t) \in \Omega_M$ and $r \leq P_m$ where r is uniformly distributed random number in $(0, 1)$ and $P_m \equiv P_m(\mathbf{x}_{i,j}(t), \mathbf{x}_{i,j}(t + \Delta t))$ was introduced in Section 1.2.2.
- For a straight interface I , the probability P_m is given by (1.9).

If the probability Ψ is strictly less than 1, then we have to incorporate into the TRM that all molecules which satisfy (a) and which are not transported to Ω_C are reflected

TABLE 1.2

The pseudocode of the TRM for stochastic reaction-diffusion simulation.

- | |
|--|
| <p>(i) Define the subdomains Ω_C and Ω_M and the interface $I = \partial\Omega_C \cap \partial\Omega_M$. Subdivide Ω_C into compartments \mathcal{C}_j, $j = 1, \dots, K$. Choose the time step Δt between updates of the molecular-based regime (M-events) in Ω_M.</p> <p>(ii) Specify the initial condition in Ω_M by placing molecules Z_i^j in Ω_M at initial positions $\mathbf{x}_{i,j}(0) \in \Omega_M$, $i = 1, 2, \dots, M$, $j = 1, 2, \dots, n(i)$, where $n(i)$ is the initial number of molecules of the i-th chemical species \mathcal{Z}_i in Ω_M.</p> <p>(iii) Specify the initial condition in Ω_C by initializing the copy numbers $\mathcal{N}_{i,j}$ in Ω_C for each chemical species \mathcal{Z}_i in each compartment \mathcal{C}_j, $i = 1, 2, \dots, M$, $j = 1, 2, \dots, K$. Initialize time as $t := 0$.</p> <p>(iv) Use equation (1.1) to calculate $t_{\mathcal{E}}$, the putative times at which all C-events \mathcal{E} will take place. Set $t_M = \Delta t$ and $t_C = \min_{\mathcal{E}} t_{\mathcal{E}}$ where the minimum is taken over all possible C-events \mathcal{E}.</p> <p>(v) If $t_C \leq t_M$, then the next C-event occurs:</p> <ul style="list-style-type: none"> • Update current time $t := t_C$. • Change the number of molecules in Ω_C to reflect the specific C-event that has occurred. If this event is one in which a molecule of chemical species \mathcal{Z}_i leaves Ω_C bound for Ω_M, then compute its initial position in Ω_M according to the probability distribution $f_{i,j}(\mathbf{x})$ and remove it from the corresponding compartment \mathcal{C}_j. • Calculate the next putative time for the current C-event by equation, (1.1). For all propensity functions $\alpha_{\mathcal{E}}$ that are changed as a result of the C-event, determine the putative times of the corresponding event by equation (1.2). • Set $t_C := \min_{\mathcal{E}}(\tau_{\mathcal{E}})$. <p>(vi) If $t_M \leq t_C$, then the next M-event occurs:</p> <ul style="list-style-type: none"> • Update current time $t := t_M$. • Change the locations of all molecules in Ω_M using equation (1.7). • Implement boundary conditions at the external boundary $\partial\Omega_M \setminus I$. • Initialize all molecules which migrated from Ω_C to Ω_M since the previous M-event at locations computed in the step (v) according to $f_{i,j}(\mathbf{x})$. • Perform all reaction events in Ω_M. • Identify all molecules that interact with the interface I from Ω_M (excluding those just initiated) using conditions (a)–(b) from Section 1.3.2. Move each molecule into the appropriate compartment in Ω_C with probability Ψ. Otherwise, its position is reflected back to Ω_M. • For all propensity functions $\alpha_{\mathcal{E}}$ that are changed as a result of the M-event determine the putative times of the corresponding C-event by equation (1.2). • Update $t_M := t_M + \Delta t$ and, if necessary, set $t_C := \min_{\mathcal{E}}(\tau_{\mathcal{E}})$. <p>(vii) Repeat steps (v) and (vi) until the desired end of the simulation.</p> |
|--|

back to Ω_M . However, this condition is not necessary in 1D where it is possible to prove that $\Psi = 1$ [11]. This simplifies the implementation of the TRM in 1D. In the next section, we summarize the results of the 1D theory presented in [11]. Then, in Section 2, we analyse the TRM in 2D.

1.3.3. Summary of analysis of the TRM in 1D. In [11], the TRM is presented and analysed in a one dimensional domain $\Omega = (-\infty, \infty)$ which was divided by the interface $I = \{0\}$ into $\Omega_C = (-\infty, 0)$ and $\Omega_M = (0, \infty)$. The subdomain Ω_C was divided into compartments of the same length h , i.e. $\mathcal{C}_j = (-jh, (1-j)h)$, $j = 1, 2, \dots$. In this case, there is only one interfacial compartment corresponding to $j = 1$ and coordinates $x \in \Omega_M$ are defined as the displacement from the interface I . It was obtained that

$$\Phi_{i,1} = \frac{2h}{\sqrt{\pi D_i \Delta t}}, \quad \Psi = 1, \quad (1.11)$$

$$f_{i,1}(x) = \sqrt{\frac{\pi}{4D_i \Delta t}} \operatorname{erfc}\left(\frac{x}{\sqrt{4D_i \Delta t}}\right), \quad x \in \Omega_M, \quad (1.12)$$

where $\operatorname{erfc}(x) = 2/\sqrt{\pi} \int_x^\infty \exp(-t^2)dt$ is the complementary error function. These formulae were derived under the assumption $D\Delta t \sim h^2$ as $h \rightarrow 0$, a condition which is used throughout the manuscript. If Δt gets larger than this then the expected jump distance of molecules in the Brownian domain, $\sqrt{2D\Delta t}$, becomes greater than the compartment size h . Since in the simplest form of the TRM scheme we do not allow Brownian particles to jump to interior compartments (particles that cross the interface are placed in a boundary compartment), we often assume $D\Delta t < h^2$ (we are usually interested in a finer resolution in the Brownian domain than the compartment domain). If $D\Delta t$ is chosen much smaller than h^2 then the coupling between domains is still accurate in one dimension. However, we will see that choosing $\sqrt{2D\Delta t} \ll h$ in higher dimensions can create some numerical artefacts associated with molecules diffusing along the interface I .

2. Main results. In the rest of this paper we wish to derive forms for $\Phi_{i,j}$, Ψ and $f_{i,j}(\mathbf{x})$ in domains with dimensions greater than $N = 1$. Since these parameters, the sole requirements for the correct spatial coupling of regions Ω_C and Ω_M , are independent of the parameters for reactions we do not need to note the chemical species in our analysis. We shall therefore drop the index i and relabel D_i as D which will denote the diffusion constant for the chemical species in question. We therefore wish to find the parameters Φ_j , Ψ and $f_j(\mathbf{x})$ for domains that have more than one dimension. We shall limit the analysis to regularly spaced square compartments of length h for dimension $N = 2$, but the results can be easily generalized to regularly spaced N -dimensional cubic compartments (see Section 2.3). The parameters will be derived for a flat interface I and then we will discuss the case where I may have a corner.

2.1. Matching at a flat interface in 2D. The considered geometry is represented graphically in Figure 2.1. We present here a derivation to the parameters Φ_j , Ψ and $f_j(\mathbf{x})$ for the TRM applied to an infinite two-dimensional domain $\Omega = \mathbb{R}^2$ and a single flat interface I . To derive these algorithm parameters (and formulate them in a reasonably simplified form), we denote by (x, y) the Cartesian coordinates that describe domain Ω . Without loss of generality we assign Ω_M to the region defined by $x > 0$ and therefore Ω_C to the region defined by $x < 0$ (i.e. the interface I is the line $x = 0$). The compartments \mathcal{C}_j are regularly spaced squares of side length h . We find it convenient to describe the compartments by two indices such that each compartment $\mathcal{C}_{i,j}$ is assigned to the region described by $-(i+1)h < x < -ih$ and $jh - h/2 < y < jh + h/2$, where $i \in \mathbb{N}_0$ and $j \in \mathbb{Z}$. In what follows, we will denote

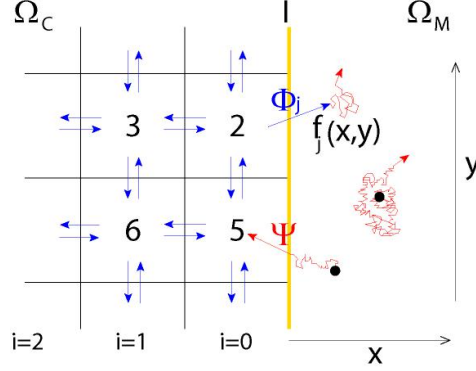


FIG. 2.1. Graphical representation of the TRM in 2D for a flat interface I . Compartment-based regime Ω_C is on the left (numbers denote the number of molecules in the corresponding compartment), molecular-based regime Ω_M on the right (three illustrative trajectories of individual molecules are plotted as red lines). The interface I is plotted as a yellow line.

by $p_{i,j}(t)h^2$ the probability of a molecule to be in the compartment $\mathcal{C}_{i,j}$, i.e. $p_{i,j}(t)$ is the (discretized, averaged) probability density in the compartment $\mathcal{C}_{i,j}$.

Since the analysis of the TRM only depends on the properties of diffusion [11], we can write the governing equations as the evolution equations for the probability density of a single diffusing molecule in Ω . The goal of the TRM is to correctly approximate its probability density function $P(x, y, t)$ where $(x, y) \in \Omega$ and time $t \geq 0$. Using equations (1.6), (1.7), (1.9), (1.10) and the description of the evolution of molecules near the interface I during the TRM, the TRM master equations for both the average probability density $p_{0,n}(t)$ for a molecule to be in the $\mathcal{C}_{0,n}$ compartment and the probability density $p(x, y, t)$ in Ω_M are given by

$$p_{0,n}(t + \Delta t) = \left(1 - \frac{(3 + \Phi_0)D\Delta t}{h^2}\right) p_{0,n}(t) + \frac{D\Delta t}{h^2} (p_{0,n-1}(t) + p_{0,n+1}(t) + p_{1,n}(t)) \\ + \frac{2\Psi}{h^2} \int_{nh-h/2}^{nh+h/2} dy \int_{-\infty}^{\infty} d\bar{y} \int_0^{\infty} d\bar{x} \int_0^{\infty} d\bar{x} p(\bar{x}, \bar{y}, t) K(x + \bar{x}) K(y - \bar{y}), \quad (2.1)$$

$$p(x, y, t + \Delta t) = \int_{-\infty}^{\infty} d\bar{y} \int_0^{\infty} d\bar{x} p(\bar{x}, \bar{y}, t) [K(x - \bar{x}) + (1 - 2\Psi)K(x + \bar{x})] K(y - \bar{y}) \\ + D\Delta t \sum_{j \in \mathbb{Z}} \Phi_j f_j(x, y) p_{0,j}(t), \quad (2.2)$$

where $K(x) = (4\pi D\Delta t)^{-1/2} \exp(-x^2/(4D\Delta t))$ is the distribution of the random displacement in the position of molecules between t and $t + \Delta t$ given by (1.7). One key assumption that is made in equation (2.1) is that molecules that are absorbed into Ω_C from Ω_M are absorbed into the closest compartment $\mathcal{C}_{0,j}$ to their position calculated at $t + \Delta t$ (see the limits of integration over the variable y in (2.1)). It can also be shown [6, 11] that the contributions of the two ways a molecule may be absorbed by the interfacial compartment (see cases (a)–(b) in Section 1.3) to the total number of absorbed molecules in a time step are equal giving rise to the factor of 2 in the integral term on the right hand side of equation (2.1) and the absorption component of the integral on the right hand side of equation (2.2).

We may further simplify equations (2.1)–(2.2) by using the symmetry of the domain in the y -direction. Firstly, since Φ_j (where now j refers to compartments $\mathcal{C}_{0,j}$ on the interface) is dependent only on the morphology of $\mathcal{C}_{0,j}$ and its relative position to I , we expect Φ_j to be independent of j and we therefore denote

$$\Phi_j \equiv \Phi. \quad (2.3)$$

Secondly, symmetry in the y -direction also allows us to make the conclusion that

$$f_j(x, y) = f_0(x, y - jh). \quad (2.4)$$

where the index of f_j refers only to interfacial compartments $\mathcal{C}_{0,j}$.

In the vicinity of $x = 0$ there is a boundary layer of width $O(\sqrt{\Delta t})$ [6, 11]. We rescale equations (2.1)–(2.2) using the dimensionless boundary layer coordinate $x = \xi\sqrt{D\Delta t}$. We also denote the probability density and placement function in this boundary layer region by $p_{\text{in}}(\xi, y, t)$ and $f_{\text{in},j}(\xi, y) = \sqrt{D\Delta t} f_j(\xi\sqrt{D\Delta t}, y)$. The rescaling of f_j is necessary to satisfy the normalisation condition

$$\int_{-\infty}^{\infty} \int_0^{\infty} f_j(x, y) \, dx \, dy = 1$$

since (as we will see) f_j vanishes outside of the boundary layer. Thus, using (2.3) and (2.4), in the boundary layer coordinates equations (2.1)–(2.2) become

$$\begin{aligned} p_{0,n}(t + \Delta t) = & \left(1 - \frac{(3 + \Phi)}{\Lambda^2}\right) p_{0,n}(t) + \frac{1}{\Lambda^2} (p_{0,n-1}(t) + p_{0,n+1}(t) + p_{1,n}(t)) \\ & + \frac{2\Psi}{h\Lambda} \int_{nh-h/2}^{nh+h/2} dy \int_{-\infty}^{\infty} d\bar{y} \int_0^{\infty} d\bar{\xi} \int_0^{\infty} d\bar{\xi} p_{\text{in}}(\bar{\xi}, \bar{y}, t) \kappa(\xi + \bar{\xi}) K(y - \bar{y}), \end{aligned} \quad (2.5)$$

$$\begin{aligned} p_{\text{in}}(\xi, y, t + \Delta t) = & \int_{-\infty}^{\infty} d\bar{y} \int_0^{\infty} d\bar{\xi} p_{\text{in}}(\bar{\xi}, \bar{y}, t) [\kappa(\xi - \bar{\xi}) + (1 - 2\Psi)\kappa(\xi + \bar{\xi})] K(y - \bar{y}) \\ & + \sqrt{D\Delta t} \Phi \sum_{j \in \mathbb{Z}} f_{\text{in},0}(\xi, y - jh) p_{0,j}(t), \end{aligned} \quad (2.6)$$

where $\Lambda = h/\sqrt{D\Delta t}$ and $\kappa(\xi) = \sqrt{D\Delta t} K(\sqrt{D\Delta t}\xi) = (4\pi)^{-1/2} \exp(-\xi^2/4)$. Let us denote $\bar{p}(y, t) = P(0, y, t)$ and $\bar{p}_x(y, t) = P_x(0, y, t)$ where $P(x, y, t)$ is the distribution which the TRM approximates (for $x \in \mathbb{R}$ and $y \in \mathbb{R}$). In order for the models to join smoothly at the interface I we require on the compartment-based side that

$$\begin{aligned} p_{0,n}(t) & \sim P(0, nh, t) = \bar{p}(nh, t), \\ p_{1,n}(t) & \sim P(-h, nh, t) = \bar{p}(nh, t) - h\bar{p}_x(nh, t) + O(h^2), \\ p_{0,n+1}(t) & \sim P(0, nh + h, t) = \bar{p}(nh + h, t), \\ p_{0,n-1}(t) & \sim P(0, nh - h, t) = \bar{p}(nh - h, t), \end{aligned} \quad (2.7)$$

while, for the molecular-based side, we require no rapid variation in the boundary layer, so that

$$\begin{aligned} p_{\text{in}}(\xi, y, t) & \sim \bar{p}(y, t) + \sqrt{D\Delta t}(\xi + C_x)\bar{p}_x(y, t) + \dots, \\ p_{\text{in}}(\xi, y, t + \Delta t) & \sim \bar{p}(y, t + \Delta t) + \sqrt{D\Delta t}(\xi + C_x)\bar{p}_x(y, t) + \dots, \end{aligned} \quad (2.8)$$

where we have allowed for a small shift C_x in which the molecular-based region “sees” the interface [11]. Similarly

$$\int_{-\infty}^{\infty} K(y - \bar{y}) \bar{p}(\bar{y}, t) d\bar{y} = \bar{p}(y, t) + O(\Delta t).$$

Substituting the expansions (2.7)–(2.8) into equations (2.5) and (2.6), using $h \sim \sqrt{D\Delta t}$ as $h \rightarrow 0$ and $\Delta t \rightarrow 0$, we obtain,

$$\begin{aligned} 0 &= -\frac{\Phi}{\Lambda^2} \bar{p}(nh, t) + \frac{1}{\Lambda^2} h \bar{p}_x(nh, t) \\ &+ \frac{2\Psi}{\Lambda} \frac{1}{\sqrt{\pi}} \bar{p}(nh, t) + \frac{2\Psi}{\Lambda} \sqrt{D\Delta t} \left(\frac{1}{2} + \frac{C_x}{\sqrt{\pi}} \right) \bar{p}_x(nh, t) + O(h^2), \end{aligned} \quad (2.9)$$

$$\begin{aligned} 0 &= -\Psi \operatorname{erfc}\left(\frac{\xi}{2}\right) \bar{p}(y, t) \\ &+ \sqrt{D\Delta t} \left(\frac{(2 - 2\Psi)}{\sqrt{\pi}} e^{-\xi^2/4} - C_x \Psi \operatorname{erfc}\left(\frac{\xi}{2}\right) + (\Psi - 1) \xi \operatorname{erfc}\left(\frac{\xi}{2}\right) \right) \bar{p}_x(y, t) \\ &+ \sqrt{D\Delta t} \Phi \sum_{j \in \mathbb{Z}} f_{\text{in},0}(\xi, y - jh) \bar{p}(jh, t) + O(h^2). \end{aligned} \quad (2.10)$$

Equating coefficients of $\bar{p}(nh, t)$ and $\bar{p}_x(nh, t)$ in (2.9) gives

$$\Phi = \frac{2\Psi\Lambda}{\sqrt{\pi}}, \quad 1 = \Psi \left(1 + \frac{2C_x}{\sqrt{\pi}} \right). \quad (2.11)$$

From the coefficient of \bar{p}_x in (2.10) we see that

$$\Psi = 1, \quad \text{and} \quad C_x = 0. \quad (2.12)$$

Consequently, equation (2.11) implies that Φ satisfies (1.11). Using (2.12) and (2.10) we find that $f_{\text{in},0}$ has to satisfy

$$\operatorname{erfc}\left(\frac{\xi}{2}\right) \bar{p}(y, t) = \frac{2h}{\sqrt{\pi}} \sum_{j \in \mathbb{Z}} f_{\text{in},0}(\xi, y - jh) \bar{p}(jh, t) + O(h^2).$$

Writing

$$f_{\text{in},0}(\xi, y) = \frac{\sqrt{\pi}}{2} \operatorname{erfc}\left(\frac{\xi}{2}\right) F(y),$$

this becomes

$$\bar{p}(y, t) = h \sum_{j \in \mathbb{Z}} F(y - jh) \bar{p}(jh, t) + O(h^2). \quad (2.13)$$

This is a standard interpolation problem. The simplest weight function which gives $O(h^2)$ accuracy is the triangle function

$$F(y) = \begin{cases} \frac{1}{h} \left(1 - \frac{|y|}{h} \right), & \text{for } -h < y < h, \\ 0, & \text{otherwise.} \end{cases} \quad (2.14)$$

Thus

$$f_0(x, y) = \begin{cases} \frac{1}{h} \sqrt{\frac{\pi}{4D\Delta t}} \operatorname{erfc}\left(\frac{x}{\sqrt{4D\Delta t}}\right) \left(1 - \frac{|y|}{h}\right), & \text{for } -h < y < h, \\ 0, & \text{otherwise.} \end{cases} \quad (2.15)$$

It is important to note that our expansions (2.7) assume that the probability $p_{i,j}$ of being in compartment $\mathcal{C}_{i,j}$ should be a continuous extension of $p(x, y)$ evaluated at $(-ih, jh)$ which is in the center of the right side of the compartments. If the expansions (2.7) were taken in the center of the compartments (evaluated at $(-ih - h/2, jh)$) the result would be that $C_1 = -\Lambda/2$ and thus a shift in the continuous expected probability density curve over the interface is seen resulting in an apparent error of $h\bar{p}_x/2 + O(h^2)$ as $\Delta t \rightarrow 0$ on the interface [11]. This error can therefore be reduced by refining the compartments near the interface (remembering that this might mean also reducing Δt such that $D\Delta t \sim h^2$).

The derivation above was conducted under the assumption $D\Delta t \sim h^2$. Let us now assume $D\Delta t \ll h^2$ instead. Then $\Lambda = h/\sqrt{D\Delta t}$ and Φ (given by (1.11) as $2\Lambda/\sqrt{\pi}$) are no longer of order 1, and the above derivation may fail. In particular, we retain terms of order h while ignoring terms of order Φh^2 . If we are interested in very small Δt the errors associated with this mismatch between Δt and h may be reduced by replacing $F(y)$ by the step function

$$\bar{F}(y) = \begin{cases} \frac{1}{h}, & \text{for } -h/2 < y < h/2, \\ 0, & \text{otherwise,} \end{cases} \quad (2.16)$$

which gives $O(h)$ accuracy to (2.13). This function is also easier to implement in the case of corners which will be discussed in the next section. Using (2.16) instead of (2.14), equation (2.15) reads as follows

$$f_0(x, y) = \begin{cases} \frac{1}{h} \sqrt{\frac{\pi}{4D\Delta t}} \operatorname{erfc}\left(\frac{x}{\sqrt{4D\Delta t}}\right), & \text{for } -h/2 < y < h/2, \\ 0, & \text{otherwise.} \end{cases} \quad (2.17)$$

These issues will be discussed further in Section 3.

2.2. Interface corners. The analysis in the previous section does not extend trivially to the case when there are corners in the interface I . Indeed, when the interface is not perfectly flat the previous section is invalid. However, since we are restricting our analysis to regular cubic lattices in Ω_C , the interface must be made up of a series of straight edges connected at right angles. Let us consider the compartments $\mathcal{C}_{i,j}$ assigned to the region $((i-1)h, ih) \times ((j-1)h, jh)$, where the indices $(i, j) \in \mathbb{Z} \times \mathbb{Z} \setminus \mathbb{N} \times \mathbb{N}$ (i.e. they fill the complement of the positive quadrant). The considered geometry is represented graphically in Figure 2.2(a).

Molecules cannot leave compartment $\mathcal{C}_{0,1}$ using (2.14). This is because there is a non-zero probability that the molecule crosses diagonally to the region of $\mathcal{C}_{1,0}$ and vice versa. This diagonal movement is prohibited by the rules of the compartment region but is allowed in the molecular region. Furthermore, molecules in Ω_M may move into $\mathcal{C}_{0,0}$ during one time step. Typically, molecules in compartments will not be able to move diagonally out of $\mathcal{C}_{0,0}$. Whilst it may be possible to make diagonal motion an exception for $\mathcal{C}_{0,0}$, atypical functions placing molecules into Ω_M from $\mathcal{C}_{0,0}$,

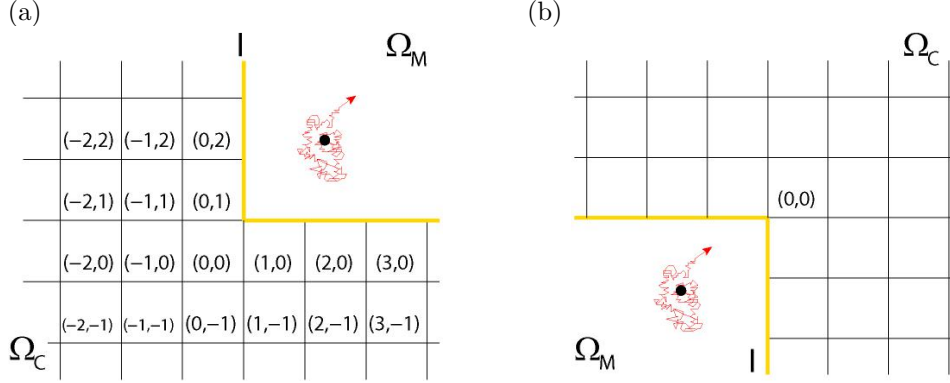


FIG. 2.2. (a) Illustration of corner geometry in two-dimensions. Compartment indices are denoted as in Section 2.2. (b) The corner geometry used in illustrative numerical simulations in Section 3.2.

$\mathcal{C}_{0,1}$ and $\mathcal{C}_{1,0}$ must be determined and also rules for how molecules in Ω_M close to the corner migrate diagonally, left or down into Ω_C must be determined. It is important to note that the added complexity to these corner compartments is not trivial like the case when the compartments form a straight interface. If we attempted to generalize (2.14), then complex distributions would have to be sampled from to place molecules from $\mathcal{C}_{0,1}$ and $\mathcal{C}_{1,0}$ into Ω_M and several tests would have to be performed on molecules in Ω_M (to see if they meet criteria for diagonal migration into Ω_C , or to determine if they move down or left over the interface). Given this complication, we find it reasonable to use (2.16) instead of (2.14) which means that we use (2.17) instead of (2.15). Distribution (2.17) does not allow for molecules to leak between $\mathcal{C}_{0,1}$ and $\mathcal{C}_{1,0}$ but at the cost of accuracy in the local region around the corner.

The treatment of molecules at the corner is therefore described by the following rules. Molecules in compartments $\mathcal{C}_{0,1}$ and $\mathcal{C}_{1,0}$ have the propensities given by (1.10), namely

$$\Phi \frac{D}{h^2} \mathcal{N}_{0,1}, \quad \Phi \frac{D}{h^2} \mathcal{N}_{1,0},$$

where $\mathcal{N}_{0,1}$ (resp. $\mathcal{N}_{1,0}$) is the number of molecules in the compartment $\mathcal{C}_{0,1}$ (resp. $\mathcal{C}_{1,0}$). Molecules from $\mathcal{C}_{0,0}$ may not enter Ω_M directly. Molecules from Ω_M that land in $\mathcal{C}_{0,0}$ or satisfy condition (b) in Section 1.3.2 for both parts $\{x = 0\}$ and $\{y = 0\}$ of the interface I are placed at random (with probability 1/2) in $\mathcal{C}_{1,0}$ or $\mathcal{C}_{0,1}$. Molecules in the compartment $\mathcal{C}_{0,1}$ migrating to Ω_M are placed according to the distribution (2.17). Molecules in the compartment $\mathcal{C}_{1,0}$ migrating to Ω_M are placed according to the distribution

$$f_0(x, y) = \begin{cases} \frac{1}{h} \sqrt{\frac{\pi}{4D\Delta t}} \operatorname{erfc}\left(\frac{y}{\sqrt{4D\Delta t}}\right), & \text{for } -h/2 < x < h/2, \\ 0 & \text{otherwise,} \end{cases} \quad (2.18)$$

which can be obtained from the distribution (2.17) by exchanging the variables x and y . Thus, in both cases, we use (1.12) perpendicular from their respective interfaces and the step distribution (2.16) tangentially along each respective interface.

Since $D\Delta t < h^2$ molecules that are in compartments $\mathcal{C}_{i,0}$ and $\mathcal{C}_{0,j}$ ($i, j \geq 2$) are not significantly affected by the corner within one time step. We therefore use the

probability distribution (2.17) for these compartments. Thus we use the distribution (2.16) for molecules leaving the corner compartments, and the triangle distribution (2.14) for molecules leaving all other boundary compartments.

Finally, we note that we also tested the alternative of using a one-sided triangle distribution for the corner compartments $\mathcal{C}_{1,0}$ or $\mathcal{C}_{0,1}$. It produced results which were indistinguishable numerically from the distribution (2.16), although this one-sided distribution includes a small bias of particles away from the corner.

2.3. Parameters for a flat interface in N dimensions. The derivation presented in Section 2.1 can be used for flat interfaces in arbitrary dimensions. One can show that the parameters $\Phi_j = \Phi$ and Ψ are independent of the number of dimensions N of the domain for a flat interface with a regular cubic compartment arrangement in Ω_C (and therefore take the values derived in Section 2.1). Furthermore one can show that the distribution $f_0(\mathbf{x})$ for placing molecules in Ω_M is the product of N distributions separating the coordinates

$$f_0(x_1, x_2, \dots, x_N) = F^\perp(x_1) \prod_{i=2}^N F^\parallel(x_i). \quad (2.19)$$

Here, the distribution $F^\perp(x_1)$ is for the coordinate x_1 perpendicular to the interface $I = \{x_1 = 0\}$. It is given (see equations (1.12) and (2.15)) by

$$F^\perp(x_1) = \sqrt{\frac{\pi}{4D\Delta t}} \operatorname{erfc}\left(\frac{x_1}{\sqrt{4D\Delta t}}\right). \quad (2.20)$$

The remaining $N - 1$ identical distributions for each coordinate x_i , $i = 2, \dots, N$, tangential to the interface I , are denoted as $F^\parallel(x_i)$ in equation (2.19). If the origin is placed at the center of compartment in question, then one can follow the derivation presented in Section 2.1 to obtain $F^\parallel(x_i) = F(x_i)$ given by (2.14). Equation (2.19) indicates that tangential coordinates should be chosen independently from each other.

3. Illustrative numerical examples. In this section we present simple diffusion simulations using the TRM to demonstrate its accuracy and convergence. We will compare results computed by distributions (2.15) and (2.17).

3.1. Straight interface. We will consider a diffusing molecule which starts at the origin at (dimensionless) time $t = 0$ and diffuse with (dimensionless) diffusion constant $D = 1$ in the semi-infinite two-dimensional domain $\Omega = (0, \infty) \times (0, \infty)$. Boundary $\partial\Omega$ will be considered reflective.

The probability distribution, $P(x, y, t)$, to find the molecule at time t given its initial position at the origin evolves according to the partial differential equation (PDE)

$$\frac{\partial P}{\partial t} = \frac{\partial^2 P}{\partial x^2} + \frac{\partial^2 P}{\partial y^2}, \quad (3.1)$$

with the initial condition $P(x, y, 0) = \delta(x, y)$ where δ is the Dirac delta function. Using no-flux (reflective) boundary condition ($\nabla P \cdot \hat{\mathbf{n}} = 0$), equation (3.1) can be solved as

$$P(x, y, t) = \frac{1}{\pi t} \exp\left(\frac{-(x^2 + y^2)}{4t}\right). \quad (3.2)$$

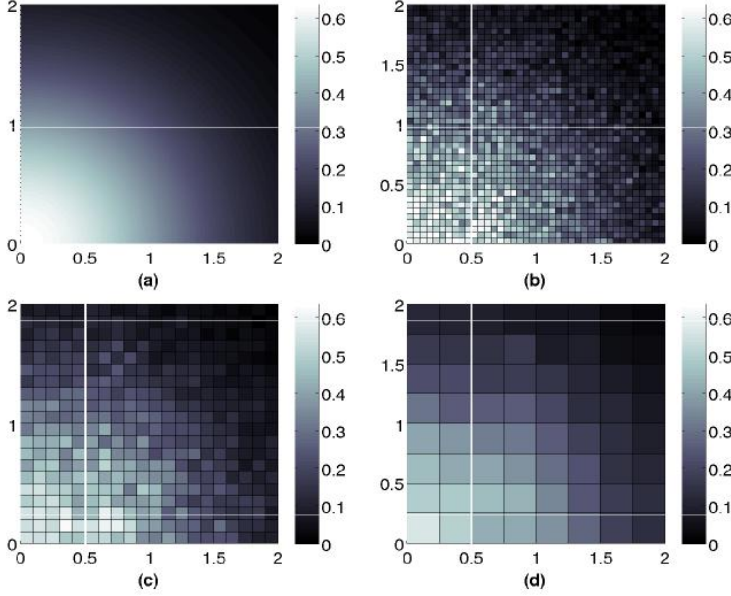


FIG. 3.1. Probability distribution at time $t = 0.5$ estimated using $N_0 = 2 \times 10^5$ realisations of the TRM method for the domain partition (3.3). (a) The expected distribution found by (3.2). (b) TRM simulation with compartment size $h = 0.05$ and $\Delta t = 0.0004$. (c) TRM simulation with compartment size $h = 0.1$ and $\Delta t = 0.0016$. (d) TRM simulation with compartment size $h = 0.25$ and $\Delta t = 0.01$. Ω_C can be seen in (b)-(d) on the right and Ω_M to the left of the white solid line. These simulations were done using sampling (2.15).

We shall simulate this diffusion process stochastically using the TRM where Ω is divided into

$$\Omega_M = (0, 0.5) \times (0, \infty) \quad \text{and} \quad \Omega_C = (0.5, \infty) \times (0, \infty). \quad (3.3)$$

We run $N_0 = 2 \times 10^5$ realizations of the TRM for the molecule starting at the origin and note its state (either in the molecular regime or compartment regime) at each time step until $t = 1$. We simulate the compartment regime using a square lattice with non-dimensional compartment spacings $h = 0.05$, $h = 0.1$ and $h = 0.25$. Since our analysis uses the assumption $D\Delta t \sim h^2$, we use the time steps $\Delta t = 0.0004$, $\Delta t = 0.0016$ and $\Delta t = 0.01$ respectively with $D = 1$ such that $h/\sqrt{D\Delta t} = 2.5 \sim O(1)$.

At $t = 0.5$ the molecule positions (for each realisation) are binned according to their compartment (or in the case of the molecular regime, counted in bins of area h^2) and a plot of these bin copy numbers divided by $N_0 h^2$ is produced to show the approximate probability density that is generated by the TRM. These probability densities are shown for comparison against the exact solution (3.2) in Figure 3.1 for each compartment size h . The distributions generated using the TRM match well with the expected distribution and appear to be more accurate as h is decreased.

To better visualize the accuracy of the TRM, we define the error function

$$\text{Error}(t) = \frac{C_{TRM}(t)}{N_0} - \iint_{\Omega_C} P(x, y, t) \, dx \, dy, \quad (3.4)$$

where $C_{TRM}(t)$ is the number of realisations of the TRM which have the molecule positioned in Ω_C at time t . Therefore, the fraction $C_{TRM}(t)/N_0$ is the approximation of

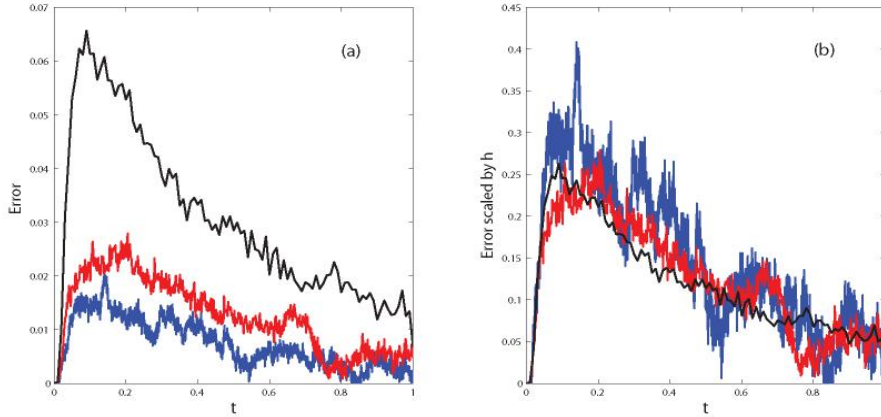


FIG. 3.2. (a) The error of the TRM defined by (3.4) for $h = 0.05$ and $\Delta t = 0.0004$ (blue line), $h = 0.1$ and $\Delta t = 0.0016$ (red line) and $h = 0.25$ and $\Delta t = 0.01$ (black line). TRM simulations are taken with $\Omega_C = (0.5, \infty) \times (0, \infty)$ and $\Omega_M = (0, 0.5) \times (0, \infty)$. These simulations were done using sampling (2.15). (b) Results from panel (a) scaled by h .

$\iint_{\Omega_C} P(x, y, t) dx dy$ and the error (3.4) measures the accuracy of this approximation.

In Figure 3.2(a) we present the error (3.4) as a function of time for the $h = 0.05$, $h = 0.1$ and $h = 0.25$ simulations. There is a maximum in this error around $t \sim 0.1$ for all simulations. The predicted error on the boundary (see Section 2.1) is proportional to the net flux over the interface ($h\bar{p}_x/2 + O(h^2)$). We note that this flux reaches a maximum (according to the exact solution (3.2)) at around $t = 1/24$. The reason why the maximum of our measured error does not match up with this time is because the error at the interface is described by a small discontinuity in the distribution on the boundary, this discontinuity then diffuses into each of the subdomains. After $t = 1/24$ the discontinuity is reduced, thereby reducing this bias effect but there is still some time before the distributions are corrected by diffusion. It is for this reason that coupling at the interface correctly is so crucial. A small bias in the flow over the interface in one direction can lead to an avalanching effect on the distribution. Whilst the TRM cannot eliminate the error that is associated with changing of regime entirely, it does optimize the error. We also expect the error, however, to be proportional to h . We can see that this is the case by plotting the error (3.4) divided by h for each simulation (Figure 3.2(b)). Each of the three curves in Figure 3.2(b) approximately overlay implying that the leading order term of the error is $O(h)$. This means that in the continuous limit $h \rightarrow 0$ the error that is due to the TRM approximately converges linearly with h , as expected.

The purpose of the TRM is to match the concentration and perpendicular flux of molecules at the boundary in the most optimal way given small h and small Δt . In our analysis, we restricted the algorithm parameters to the case $D\Delta t \sim h^2$. In some applications, this might not be a preferred parameter regime because Δt determines the resolution of the microscopic region Ω_M and if $D\Delta t \sim h^2$ then this resolution is no better than the compartment-based regime. One must be careful in this case since for $D\Delta t \ll h^2$, the parameter $\Phi = 2\Lambda/\sqrt{\pi}$ (defined by (2.11)) may become significantly larger than 1. Previously, higher order terms of the form Φh^2 in (2.9)–(2.10) (which were ignored as “too small”) now become dominant over terms that are of the order

of h . This manifests itself into an increase in the dispersion inside the boundary layer near the interface in the tangential direction. This effect can be seen in Figure 3.3(c).

The increase in the dispersion in the tangential direction may also be explained by following the TRM mechanism. Consider molecules in Ω_M close to the interface between Ω_M and Ω_C . If these molecules are sufficiently close to the interface, they are likely to be absorbed into a compartment in Ω_C . To compensate for this rapid absorption of molecules, the compartments on the interface must return these molecules to the boundary layer at comparable rates. Since, as $\Delta t \rightarrow 0$, the boundary layer gets thinner, this increases the rate of resorption of molecules having just come from Ω_C . If a molecule enters an interfacial compartment $\mathcal{C}_{0,j}$ near the boundary to the adjacent compartment $\mathcal{C}_{0,j-1}$ then this molecule effectively jumps a distance $h/2$ in the tangential direction (because its position in Ω_C can be considered as the center of $\mathcal{C}_{0,j}$). This molecule is then rapidly interchanged between Ω_M and $\mathcal{C}_{0,j}$ each time with a new tangential coordinate until the tangential coordinate falls out of line with \mathcal{C}_j or the molecule diffuses away from the interface. The former of these two options occurs more often if Δt is small since the tangential coordinate is rapidly resampled until the 0.25 chance of being sampled outside the compartment \mathcal{C}_j is realized if we use (2.14). In these situations, it is better to use (2.16) for the tangential coordinate. This is because, (2.16) restricts the molecule initiation to the compartment from which it came. Furthermore, one can reduce this effect by reducing the size of h . Reducing h helps to reduce Φ .

It is possible to show that this numerical artefact is improved, if h cannot be reduced, by using step function (2.16) instead of triangle function (2.14) to sample molecule positions tangentially to the interface. However, if $D\Delta t \sim h^2$ then (2.14) offers the best results. This is demonstrated in Figure 3.3. In Figure 3.3, the least amount of artificial dispersion is achieved if $D\Delta t \sim h^2$ using the triangle function sampling (2.14) but the triangle function sampling introduces more severe artificial dispersion along the interface than step function sampling (2.16) if $D\Delta t \ll h^2$.

3.2. Interface with a corner. To demonstrate that the TRM produces good results when there is a corner in the interface, we present also the results of TRM simulations of the same problem as in Section 3.1 with subdomains redefined as follows

$$\Omega_M = (0, 0.5) \times (0, 0.5), \quad \Omega_C = (0, 0.5) \times (0.5, \infty) \cup (0.5, \infty) \times (0, \infty). \quad (3.5)$$

The details of the TRM implementation of corners are discussed in Section 2.2. The corner is oriented as in Figure 2.2(b), i.e. the TRM implementation presented in Section 2.2 for the corner orientation in Figure 2.2(a) is adjusted (by a simple rotation) to the corner orientation in Figure 2.2(b).

In Figure 3.4 we present the distributions that result using the TRM for the domain partition (3.5). These distributions are calculated in the same way as those distributions found in Figure 3.1. The distributions are plotted, similarly, at $t = 0.5$. There is good agreement with the expected distribution (Figure 3.4(a)) especially for small h . In Figure 3.5(a), we present the error (3.4) as a function of time for the $h = 0.05$, $h = 0.1$ and $h = 0.25$ simulations. To verify that the error due to the TRM is still $O(h)$ when the interface has a corner in it, Figure 3.5(b) shows the error for the TRM simulations scaled by h .

In Figure 3.6(a), we again see the artefact for small Δt in the compartment described by the region $x \in [0.5, 0.75)$, $y \in [0.5, 0.75)$; an unexpectedly large number of molecules. This is because diffusion is biased tangentially along both sides of the

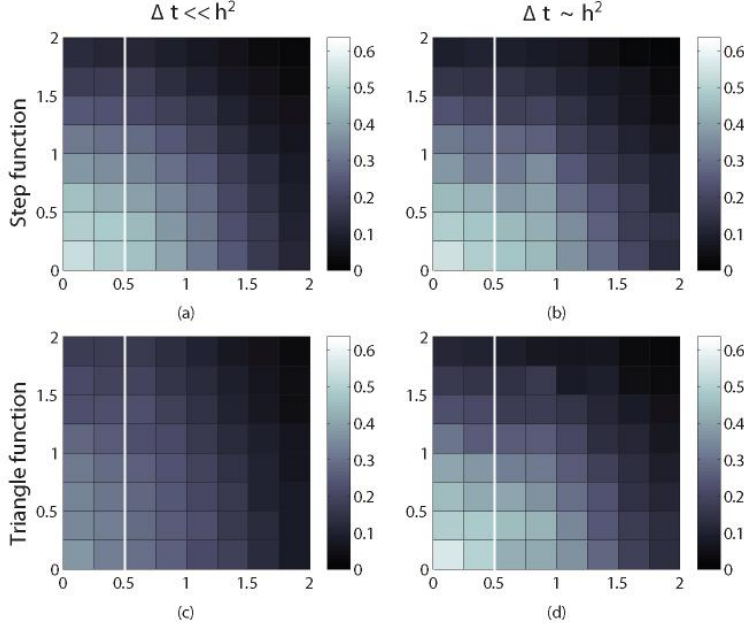


FIG. 3.3. Probability distribution at time $t = 0.5$ estimated using $N_0 = 2 \times 10^5$ realisations of the TRM method for the domain partition (3.3). In all simulations $h = 0.25$ and $D = 1$. Ω_C can be seen in (a)-(d) on the right and Ω_M to the left of the white solid line denoting interface I . TRM simulations with (a) $D\Delta t = 10^{-5} \ll h^2$ and (2.15); (b) $D\Delta t = 0.01 \sim h^2$ and (2.15); (c) $D\Delta t = 10^{-5} \ll h^2$ and (2.17); (d) $D\Delta t = 0.01 \sim h^2$ and (2.17).

interface (due to the large h and small Δt as we discussed in Section 3.1) and these molecules gather at the corner.

4. Discussion. In this paper we presented an analysis of the TRM on regular lattices in dimensions larger than one. We have derived TRM parameters to simulate diffusing molecules migrating over interface I that separates domain Ω_C in which molecules are constrained to a lattice and domain Ω_M whereby molecules can diffuse in continuous space. The TRM algorithm is presented in Table 1.2. We considered two cases $D\Delta t \ll h^2$ and $D\Delta t \sim h^2$. We showed that the parameter $\Phi_{i,j}$ defined in (1.10) can be chosen as in the one-dimensional case (1.11). The distribution $f(\mathbf{x})$ for placing molecules in Ω_M was presented in equation (2.19). In particular, each tangential direction to the interface may be treated independently and in the same way. We presented two different approaches (2.14) and (2.16) for sampling tangential directions.

In the case $D\Delta t \ll h^2$, the step function approximation (2.16) is the most appropriate choice. In particular, the distribution for placing molecules in Ω_M is given by (2.17) for two-dimensional problems. In the case $D\Delta t \sim h^2$, the triangle function approximation (2.14) is the most appropriate choice, i.e. the distribution for placing molecules in Ω_M is given by (2.15). Moreover, Figure 3.3 demonstrates that the overall best results (in terms of accuracy) can be obtained in the case $D\Delta t \sim h^2$ and (2.14). However, imposing the condition $D\Delta t \sim h^2$ over the whole domain Ω_C might lead to computationally intensive simulations. A natural solution to this problem would be

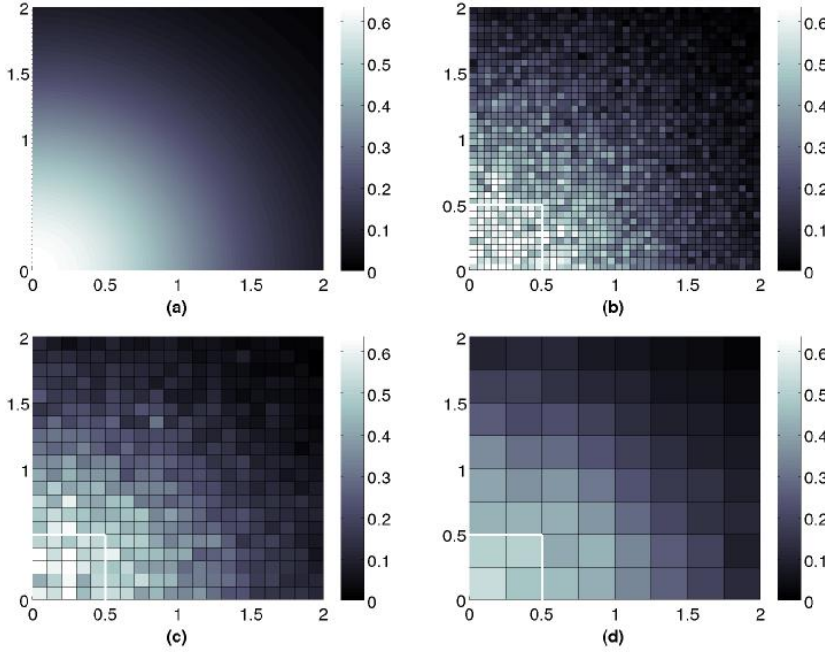


FIG. 3.4. Probability distribution at time $t = 0.5$ estimated using $N_0 = 2 \times 10^5$ realisations of the TRM method for the domain partition (3.5). (a) The expected distribution found by the exact solution (3.2). (b) TRM simulation with compartment size $h = 0.05$ and $\Delta t = 0.0004$. (c) TRM simulation with compartment size $h = 0.1$ and $\Delta t = 0.0016$. (d) TRM simulation with compartment size $h = 0.25$ and $\Delta t = 0.01$. Ω_C can be seen in (b)-(d) outside of Ω_M which is boxed by the white solid line (interface I) about the origin. These simulations were done using sampling (2.17)–(2.18) near the corners according to the approach described in Section 2.2.

to use unstructured meshes [5] where compartments can be of different sizes. Then we could impose the condition $D\Delta t \sim h^2$ for compartments close the interface I (to maximise accuracy) and the condition $D\Delta t \ll h^2$ for compartments further from the interface (to maximise efficiency).

The last decade has seen a number of different algorithms appear in the scientific literature with the purpose of coupling two domains in space with different modelling techniques for reaction-diffusion processes similar to that of the TRM. Some of these algorithms aim to couple mesoscopic stochastic simulations on a lattice (compartment-based model) with a deterministic PDE-based mean-field description [1, 13, 30, 25]. Most of these algorithms include the use of an overlap region and use this overlap region to calculate the flux of molecules (and other conserved physical quantities) that are flowing between the two regimes. This flux is calculated by particle counting and matched to the flux condition which forms the boundary condition of the deterministic macroscopic approach [1, 13, 30, 25]. New particles are created either in a new compartment corresponding to a lattice-point used in the PDE solver that is implemented on the deterministic side of the interface (“handshaking region”) [1] or in the closest compartment to the position at which the deterministic region terminates [13, 30]. Whilst these approaches often have a region of overlap where the description of particles is transitioning from deterministic to compartment-based, these regions are typically thin and transition between the descriptions is clearly defined in space.

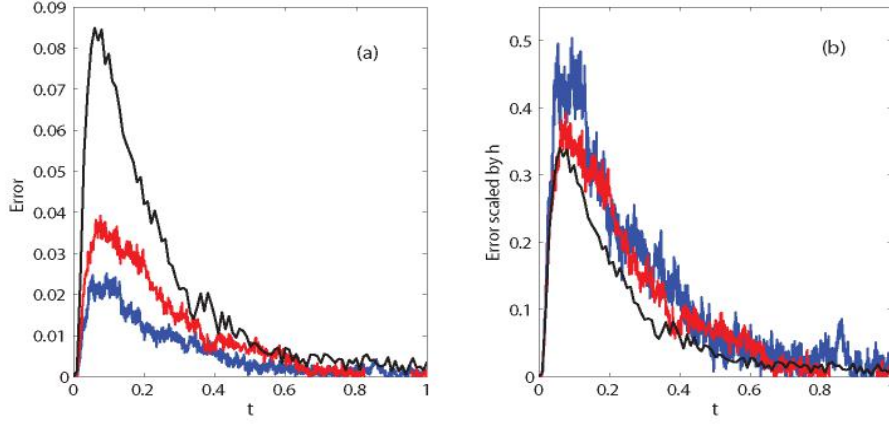


FIG. 3.5. (a) The error of the TRM defined by (3.4) for $h = 0.05$ and $\Delta t = 0.0004$ (blue line), $h = 0.1$ and $\Delta t = 0.0016$ (red line) and $h = 0.25$ and $\Delta t = 0.01$ (black line). TRM simulations are taken with Ω_M and Ω_C defined in (3.5). (b) Results from (a) scaled by h .

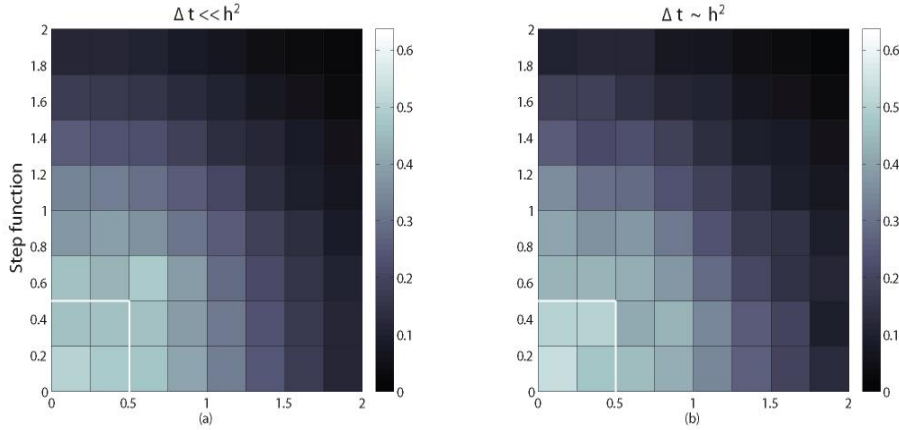


FIG. 3.6. Probability distribution at time $t = 0.5$ estimated using $N_0 = 2 \times 10^5$ realisations of the TRM method for the domain partition (3.5). In both simulations $h = 0.25$ and $D = 1$. Ω_C can be seen outside of Ω_M which is boxed by the white solid line denoting interface I . TRM simulations with (a) $D\Delta t = 10^{-5} \ll h^2$; (b) $D\Delta t = 0.01 \sim h^2$. These simulations were done using sampling (2.17)–(2.18) near the corners according to the approach described in Section 2.2.

Ferm *et al.* [10] presented a new technique for connecting deterministic regions with mesoscopic regions using a smoother coupling technique. Their technique involves interfacing a region of deterministic description with a stochastic description modelled using a tau leaping algorithm. The tau leaping algorithm is a quick compartment-based algorithm that does not account for all events as they occur but rather updates the system at discrete moments in time τ [18]. This stochastic simulation technique is fast but is only accurate if the concentration of molecules is large enough that individual events on smaller time scales produce small perturbations that do not affect the simulation significantly. This tau leaping algorithm is then interfaced with a more accurate compartment-based algorithm as the concentration drops.

Geyer *et al.* [15, 19] developed a method for coupling a deterministic numerical solution to a reaction-diffusion PDE with a Brownian dynamics molecular-based algorithm. In a similar way to the previous algorithms which couple deterministic PDEs and compartment-based algorithms the flux is determined at the interface. Molecules are initiated in the molecular-based algorithm in one-dimension using the same distribution that is stated in this manuscript (1.12) (see (11) in [15]). Indeed this boundary condition is generated by considering a “compartment” with a particular expected number of molecules. Absorption of molecules at the interface is done without consideration of condition (b) in Section 1.3.2. Since this condition is necessary in the TRM to generate the correct expected flux on both sides, the matching of the flux is instead forced manually by the algorithm. Unlike the algorithm presented in [15] the TRM couples two stochastic simulations. In the case of the TRM, the expected flux cannot be calculated without averaging over time. We present the TRM specifically with rules that govern each molecule as they cross the interface rather than try to introduce conditions that depend on the simulation itself. This is a more natural methodology since it should not be the case that an individual molecule is influenced by the net flux but rather be treated independently from each other.

Franz *et al.* [14] recently developed a technique for coupling deterministic PDEs with microscopic molecular-based simulations. Whilst this technique is different from the TRM as it interfaces a deterministic PDE-based description with a stochastic one, it deserves special mention because unlike other techniques that couple deterministic systems with stochastic simulations it does not use an averaging technique to determine the flux over the interface. Rather, it treats each particle as an individual as it crosses from the molecular-based simulation and is added to the deterministic description in a probabilistic sense, where the probability for finding the particle is known from the simulation. Transversely, molecules may migrate back when they are sampled from the probability distribution which is proportional to the continuous distribution of particles.

An algorithm similar to the TRM was recently published by Klann *et al.* [22]. In this algorithm, compartment-based and molecular-based regions are coupled. Klann *et al.* [22] present no comparison with the TRM and it is not clear how exactly they couple different regimes. However, several differences between their approach and the TRM can be identified.

The analysis presented in [11] and in Section 2 reveals that some steps of the Klann *et al.* hybrid method [22] are not optimal. For example, in [22], a molecule migrates from the compartment-based algorithm with a propensity which is natural for the lattice. This means that they have taken a value of $\Phi = 1$ instead of Φ given by (1.11). Instead of placing the molecule with a distribution given by (2.15) into the molecular-based domain they place the molecule within the compartment that corresponds with a natural extension of the compartment-based approach. Furthermore, molecules are transferred back into compartment-based molecules without the condition (b) in Section 1.3.2 (this corresponds to a value of $\Psi = 1/2$ instead of Ψ given by (1.11)). It is our experience that somewhat ad hoc or heuristic coupling of this type between compartment-based and molecular-based regions, despite being simpler to implement, may lead to heavy biasing of molecules especially in the case when the expected net flux over the interface is high. This biasing also depends on the relationship between Δt and h .

Acknowledgements. The research leading to these results has received funding from

the *European Research Council* under the *European Community's* Seventh Framework Programme (FP7/2007-2013)/ ERC grant agreement No. 239870. This publication was based on work supported in part by Award No KUK-C1-013-04, made by King Abdullah University of Science and Technology (KAUST). Radek Erban would also like to thank the Royal Society for a University Research Fellowship; Brasenose College, University of Oxford, for a Nicholas Kurti Junior Fellowship; and the Leverhulme Trust for a Philip Leverhulme Prize.

REFERENCES

- [1] F. ALEXANDER, A. GARCIA, AND D. TARTAKOVSKY, *Algorithm refinement for stochastic partial differential equations: I. linear diffusion*, Journal of Computational Physics, 182 (2002), pp. 47–66.
- [2] M. ANDER, P. BELTRAO, B. DI VENTURA, J. FERKINGHOFF-BORG, M. FOGlierINI, A. KAPLAN, C. LEMERLE, I. TOMÁS-OLIVEIRA, AND L. SERRANO, *SmartCell, a framework to simulate cellular processes that combines stochastic approximation with diffusion and localisation: analysis of simple networks*, Systems Biology, 1 (2004), pp. 129–138.
- [3] S. ANDREWS, *Serial rebinding of ligands to clustered receptors as exemplified by bacterial chemotaxis*, Physical Biology, 2 (2005), pp. 111–122.
- [4] S. ANDREWS AND D. BRAY, *Stochastic simulation of chemical reactions with spatial resolution and single molecule detail*, Physical Biology, 1 (2004), pp. 137–151.
- [5] S. ENGBLOM, L. FERM, A. HELLANDER, AND P. LÖTSTEDT, *Simulation of stochastic reaction-diffusion processes on unstructured meshes*, SIAM Journal on Scientific Computing, 31 (2009), pp. 1774–1797.
- [6] R. ERBAN AND S. J. CHAPMAN, *Reactive boundary conditions for stochastic simulations of reaction-diffusion processes*, Physical Biology, 4 (2007), pp. 16–28.
- [7] R. ERBAN AND S. J. CHAPMAN, *Stochastic modelling of reaction-diffusion processes: algorithms for bimolecular reactions*, Physical Biology, 6 (2009), p. 046001.
- [8] R. ERBAN, S. J. CHAPMAN, AND P. MAINI, *A practical guide to stochastic simulations of reaction-diffusion processes*. 35 pages, available as <http://arxiv.org/abs/0704.1908>, 2007.
- [9] R. ERBAN, M. FLEGG, AND G. PAPOIAN, *Multiscale stochastic reaction-diffusion modelling: application to actin dynamics in filopodia*, submitted to the *Bulletin of Mathematical Biology*, 2012.
- [10] L. FERM, A. HELLANDER, AND P. LÖTSTEDT, *An adaptive algorithm for simulation of stochastic reaction-diffusion processes*, Journal of Computational Physics, 229 (2010), pp. 343–360.
- [11] M. FLEGG, J. CHAPMAN, AND R. ERBAN, *The two-regime method for optimizing stochastic reaction-diffusion simulations*, Journal of the Royal Society Interface, 9 (2012), pp. 859–868.
- [12] M. FLEGG, S. RÜDIGER, AND R. ERBAN, *Diffusive spatio-temporal noise in a first-passage time model for intracellular calcium release*, to appear in the *Journal of Chemical Physics*, 2013.
- [13] E. FLEKKØY, J. FEDER, AND G. WAGNER, *Coupling particles and fields in a diffusive hybrid model*, Physical Review E, 64 (2001), p. 066302.
- [14] B. FRANZ, M. FLEGG, J. CHAPMAN, AND R. ERBAN, *Multiscale reaction-diffusion algorithms: PDE-assisted Brownian dynamics*, (available as <http://arxiv.org/abs/1206.5860>), to appear in the *SIAM Journal on Applied Mathematics*, 2013.
- [15] T. GEYER, C. GORBA, AND V. HELMS, *Interfacing Brownian dynamics simulations*, Journal of Chemical Physics, 120 (2004), pp. 4573–4580.
- [16] M. GIBSON AND J. BRUCK, *Efficient exact stochastic simulation of chemical systems with many species and many channels*, Journal of Physical Chemistry A, 104 (2000), pp. 1876–1889.
- [17] D. GILLESPIE, *Exact stochastic simulation of coupled chemical reactions*, Journal of Physical Chemistry, 81 (1977), pp. 2340–2361.
- [18] D. GILLESPIE, *Approximate accelerated stochastic simulation of chemically reacting systems*, Journal of Chemical Physics, 115 (2001), pp. 1716–1733.
- [19] C. GORBA, T. GEYER, AND V. HELMS, *Brownian dynamics simulations of simplified cytochrome c molecules in the presence of a charged surface*, Journal of Chemical Physics, 121 (2004), pp. 457–464.
- [20] J. HATTNE, D. FANGE, AND J. ELF, *Stochastic reaction-diffusion simulation with MesoRD*, Bioinformatics, 21 (2005), pp. 2923–2924.
- [21] S. KHOKHLOVA AND N. AGMON, *Green's function for reversible geminate reaction with volume*

- reactivity*, Journal of Chemical Physics, 137 (2012), p. 184103.
- [22] M. KLANN, A. GANGULY, AND H. KOEPPL, *Hybrid spatial Gillespie and particle tracking simulation*, Bioinformatics, 28 (2012), pp. i549–i555.
 - [23] J. LIPKOVÁ, K. ZYGALAKIS, J. CHAPMAN, AND R. ERBAN, *Analysis of Brownian dynamics simulations of reversible bimolecular reactions*, SIAM Journal on Applied Mathematics, 71 (2011), pp. 714–730.
 - [24] K. LIPKOW, S. ANDREWS, AND D. BRAY, *Simulated diffusion of phosphorylated CheY through the cytoplasm of Escherichia coli*, Journal of Bacteriology, 187 (2005), pp. 45–53.
 - [25] E. MORO, *Hybrid method for simulating front propagation in reaction-diffusion systems*, Physical Review E, 69 (2004), p. 060101.
 - [26] J. STILES AND T. BARTOL, *Monte Carlo methods for simulating realistic synaptic microphysiology using MCell*, in Computational Neuroscience: Realistic Modeling for Experimentalists, E. Schutter, ed., CRC Press, 2001, pp. 87–127.
 - [27] K. TAKAHASHI, S. TANASE-NICOLA, AND P. TEN WOLDE, *Spatio-temporal correlations can drastically change the response of a mapk pathway*, PNAS, 107 (2010), pp. 19820–19825.
 - [28] W. VAN GUNSTEREN AND H. BERENDSEN, *Algorithms for Brownian dynamics*, Molecular Physics, 45 (1982), pp. 637–647.
 - [29] J. VAN ZON AND P. TEN WOLDE, *Green’s-function reaction dynamics: a particle-based approach for simulating biochemical networks in time and space*, Journal of Chemical Physics, 123 (2005), p. 234910.
 - [30] G. WAGNER AND E. FLEKKØY, *Hybrid computations with flux exchange*, Philosophical Transactions of the Royal Society A: Mathematical, Physical & Engineering Sciences, 362 (2004), pp. 1655–1665.
 - [31] S. WILS AND E. DE SCHUTTER, *STEPS: Modeling and simulating complex reaction-diffusion systems with Python*, Frontiers in Neuroinformatics, 3 (2009), pp. 1–8.